Letter to the Editor

An explanation for the triphasic dependency of apparent diffusion coefficient (ADC) on T2 relaxation time: the multiple T2 compartments model

Yì Xiáng J. Wáng^

Department of Imaging and Interventional Radiology, Faculty of Medicine, The Chinese University of Hong Kong, Hong Kong SAR, China

Correspondence to: Yì Xiáng J. Wáng, PhD. Department of Imaging and Interventional Radiology, Faculty of Medicine, The Chinese University of Hong Kong, 30-32 Ngan Shing Street, Shatin, New Territories, Hong Kong SAR, China. Email: yixiang_wang@cuhk.edu.hk.

Submitted Jan 24, 2025. Accepted for publication Feb 18, 2025. Published online Mar 05, 2025.
doi: 10.21037/qims-2025-195
View this article at: https://dx.doi.org/10.21037/qims-2025-195

For *in vivo* diffusion weighted imaging (DWI), the apparent diffusion coefficient (ADC) has been considered to reflect tissue diffusion. ADC is calculated according to:

$$ADC = \frac{\ln\left[S(b_1)/S(b_2)\right]}{b_2 - b_1} \quad [1]$$

where b_2 and b_1 refers to a high *b*-value and a low *b*-value respectively, where S(b_2) and S(b_1) denote the image signal-intensity acquired at the high *b*-value and low *b*-value respectively. When the low *b*-value is 0, ADC is calculated according to

$$ADC = \frac{\ln\left[S(b_0)/S(b_2)\right]}{b_2} \quad [2]$$

where b_2 and b_0 refers to the high *b*-value and *b*=0 s/mm^2 respectively, where S(b_0) and S(b_2) denote the image signal-intensity acquired at the b-factor value of *b*=0 and the high *b*-value, respectively.

ADC can also be calculated using the three *b*-values (such as *b*=0, 50, 800 s/mm^2), according to the formula:

$$ADC_{3b} = -\frac{3\sum_{i=1}^{3} b_i \cdot \ln\left[S(b_i)\right] - \sum_{i=1}^{3} b_i \cdot \sum_{i=1}^{3} \ln\left[S(b_i)\right]}{3\sum_{i=1}^{3} b_i^2 - \left(\sum_{i=1}^{3} b_i\right)^2} \quad [3]$$

Where b_i is the ith b value (unit: s/mm^2), S(b_i) is the signal intensity at b_i.

Recently, we proposed that *in vivo* ADC measure is strongly associated with T2 relaxation time (T2) (1-5). T2 can be divided into short T2 band [<60 milliseconds (ms)], intermediate T2 band (60–80 ms), and long T2 band (>80 ms, all 3-T values). For the short T2 time band, there is a negative correlation between T2 and ADC. For the long T2 time band, there is a positive correlation between T2 and ADC. A tissue likely measures a low ADC if its T2 is close to 70 ms. On the other hand, a tissue is likely to measure a high ADC if its T2 is far away from 70 ms (*Figures 1-3*) (1-10). This observation initially appears to be puzzling. However, from Eq. [2], it can be seen that ADC value is high when the DWI signal difference between the *b*=0 image and the high *b*-value image is large. Thus, this phenomenon can be 'simplistically remembered' that, ADC value is high when: (I) the signal decay between *b*=0 image and high *b*-value image is fast such as the case for tissues with short T2, or (II) tissue has a very long T2 and appear high signal on *b*=0 image so that there is large amounts of signal to decay between *b*=0 image and high *b*-value image. ADC will measure a low value when tissue T2 is in the intermediate range of 60–80 ms. Note that, an application of the diffusion gradients will lead to a decrease in observed T2 for tissues, which can be interpreted as an application of diffusion gradients is associated with a longer time of echo (TE) for data acquisition (11).

^ ORCID: 0000-0001-5697-0717.

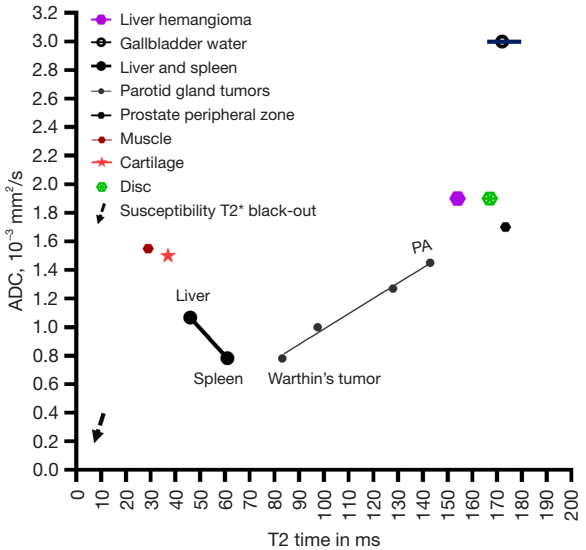

Figure 1 Relationship between T2 and ADC for various tissues, 3-T data. With parotid gland tumors, ADC from lower to higher ranking: Warthin's tumor, malignant tumor, benign tumor, PA. Note the linear correlation between T2 of parotid gland tumors and their ADC. Dotted arrow denotes susceptibility T2* black-out, which is observed with structures having a very short intrinsic T2 signal due to very short T2*. In this graph, dotted arrow is for illustration only, and does not reflect true quantitative values for susceptibility T2* black-out. This graph is adapted with permission from (4). ADC, apparent diffusion coefficient; ms, millisecond; PA, pleomorphic adenoma.

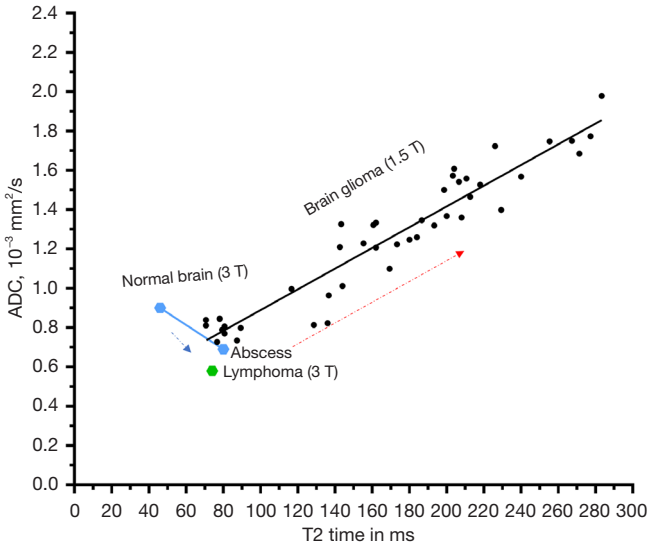

Figure 2 Relationship between T2 and ADC. Normal brain tissue and brain lymphoma are based on 3-T data (6). Brain glioma is based on 1.5-T data (7). Abscess is based on an estimation (3). The dotted blue arrow shows, as brain tissue turns into abscess or lymphoma, T2 increases and ADC decreases. The dotted orange arrow shows as glioma T2 increases, glioma ADC increases. This graph is reproduced with permission from (5). ADC, apparent diffusion coefficient; ms, millisecond.

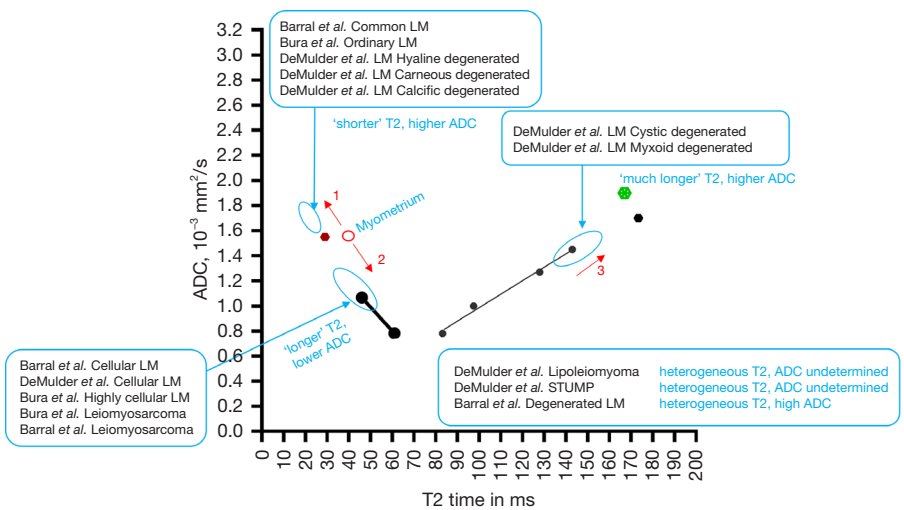

Figure 3 The T2-ADC relationship for uterine myometrium (red circle label) is considered to be at the first phase with T2 shorter than 60 ms [see (5)]. In the analyses of DeMulder *et al.* (8), Bura *et al.* (9), and Barral *et al.* (10), myometrium tumors with shorter T2 (i.e., hypointense to myometrium) are associated with higher ADC (not restricted on ADC map, blue oval and red arrow 1 in this graph), myometrium tumors with longer T2 (i.e., hyperintense to myometrium) are associated with lower ADC (restricted on ADC map, blue oval

and red arrow 2 in this graph). Cystic degenerated and myxoid degenerated tumors have very long T2 (i.e., highly hyperintense) and higher ADC (not restricted on ADC map, blue oval and red arrow 3). STUMP and lipoleiomyoma have heterogeneous T2-weighted signal and were termed as with 'undetermined ADC'. The frame of this figure is based on *Figure 1*. Data in this figure are summarized from *Tab. 2* by DeMulder *et al.* (8), *Tab. 1* by Bura *et al.* (9), and *Tab. 1* by Barral *et al.* (10). This graph is reproduced with permission from (5). ADC, apparent diffusion coefficient; LM, leiomyoma; ms, millisecond; STUMP, smooth muscle tumors of uncertain malignant potential.

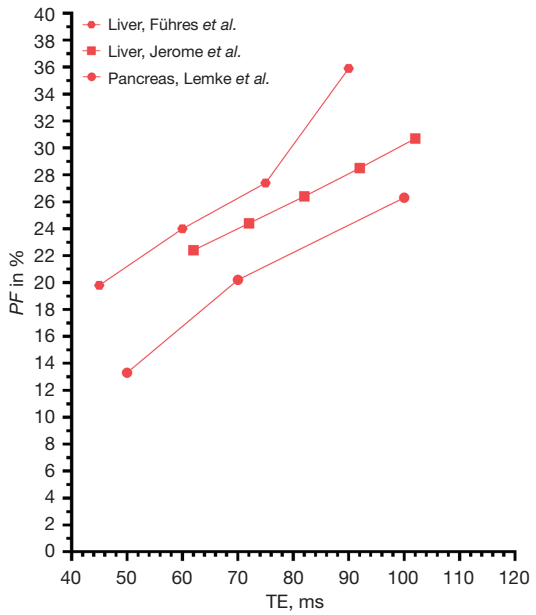

Figure 4 IVIM studies shows, if the TE is increased for DWI data acquisition which can be seen as a reduction of T2, then measured *PF* increases. Data are from Lemke *et al.* (12), Jerome *et al.* (13), and Führes *et al.* (15). DWI, diffusion weighted imaging; IVIM, Intravoxel Incoherent Motion; ms, millisecond; *PF*, perfusion fraction; TE, time of echo.

In this letter, we attempt to explain the T2 dependency of ADC with the concept of the Intravoxel Incoherent Motion (IVIM) model. The IVIM model considering the T2 effect is expressed as (11-14):

$$S(b,TE) = S_0\left[PF\cdot e^{-TE/T_2}\cdot e^{-b\cdot D_{fast}} + (1-PF)\cdot e^{-TE/T_2}\cdot e^{-b\cdot D_{slow}}\right] \quad [4]$$

where S_0 is considered a scaling term independent of both diffusion and 'T2 effect' [which is defined as magnetic resonance imaging (MRI) signal differences contributed by T2 difference], and it is implicitly assumed that repetition time is long enough to ensure no significant modulation of the signal from incomplete T1 relaxation. D_{slow} is the diffusion coefficient representing the slow 'pure' molecular diffusion (unaffected by perfusion). The perfusion fraction (*PF*) represents the fraction of the compartment related to (micro)circulation, which can be understood as the proportional 'incoherently flowing fluid' (i.e., blood) volume. D_{fast} is the perfusion-related diffusion coefficient representing the incoherent microcirculation within the voxel, which holds information for blood perfusion's speed.

A number of IVIM studies have shown that, if the TE is increased for DWI data acquisition, which can be seen as a shortening of T2 in MRI signal measurement in the transverse plane (i.e., faster signal decay, see Eq. [4]), there is an associated increase of *PF* (*Figure 4*) (12,13,15). Note that D_{fast} and *PF* are most commonly positively correlated (16). We can take it that, within a region-of-interest (ROI) or within a voxel, the T2 is not homogeneous, instead within a ROI or within a voxel there are multiple T2 elements (including T2 of arterial blood and T2 of venous blood). These T2 elements can be conceptually classified into shorter T2 elements (together referred to as 'shorter T2 compartment' in this letter) and longer T2 elements (together referred to as 'longer T2 compartment' in this letter). In *in vivo* tissues, there are likely multiple T2 compartments. There are very short T2 compartments and very long T2 compartments. For simplicity, in this letter, we only summarily consider the 'shorter T2 compartment' and 'longer T2 compartment'. From the measurement of MRI signal, shorter T2 compartment can be considered equivalent to perfusion (fast diffusion) compartment (fast initial signal decay in the IVIM model), and longer T2 compartment can be considered equivalent to diffusion compartment (*Figure 5*). For IVIM modeling, the initial fast signal decay at lower *b*-values can be due to either perfusion or due to shorter T2 elopements. Therefore, longer TE or shorter T2 is associated with increased *PF* (increased initial signal decay in the IVIM model). Hereby shorter T2 can be due to a higher portion of shorter T2 elements or the T2 relaxation times are actually shorter or a combination of both. On the other hand, an increase of T2 is associated with an increase of D_{slow} and decreased measure of the fast component [*Figure 6* (13,15,17-20), *Figure 7* (20-22), *Figure 8* (23), *Figure 9* (24-29), *Figure 10* (28,30-32)].

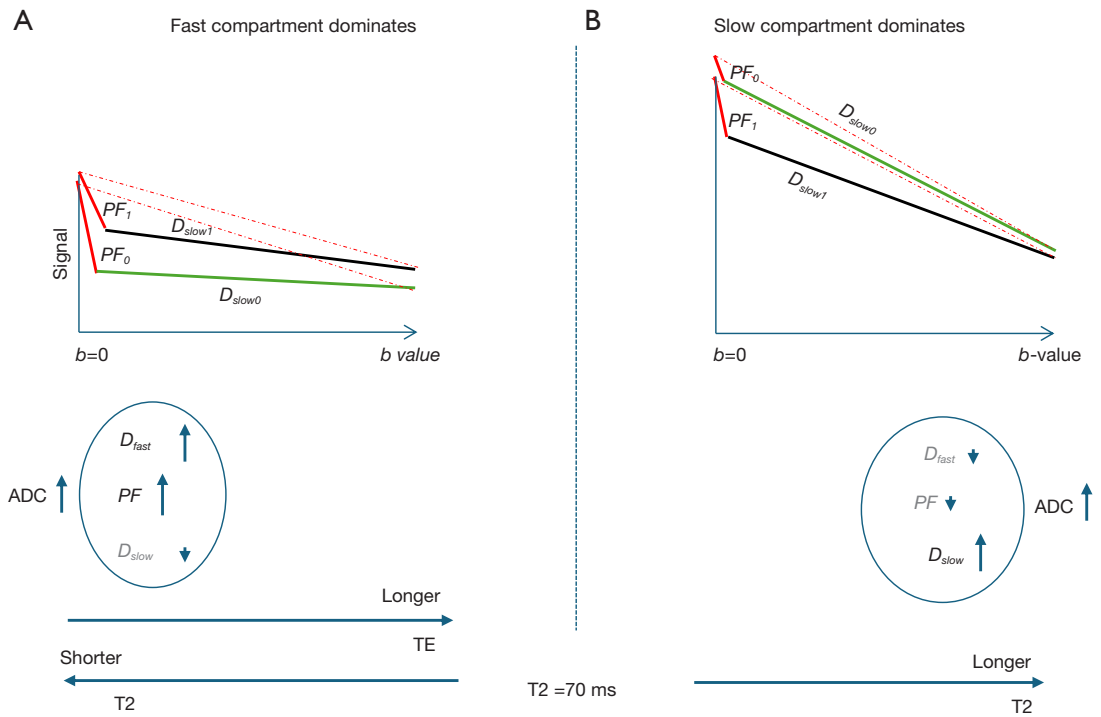

Figure 5 Considering the IVIM model, from MRI signal point of view, the shorter T2 compartment is equivalent to the perfusion compartment and the longer T2 compartment is equivalent to the slow diffusion compartment. For a tissue with an aggregate T2 value <60 ms (A), for example if T2 changes from 40 to 60 ms [such as the case of liver (PF_0) developed hepatocellular carcinoma (PF_1)], fast compartment measure decreases while slow compartment measure increases (if we do not consider other contributing factors); however, the decreased measure of the fast compartment dominates and the net effect for the composite ADC is a decrease measure. For a tissue with aggregate T2 value >80 ms (B), for example if T2 changes from 170 to 90 ms [such as the case for the prostate peripheral zone (PF_0) developed prostate cancer (PF_1)], fast compartment measure increases while slow compartment measure decreases (if we do not consider other contributing factors); however, the decrease measure of the slow compartment dominates and the net effect for ADC is a decrease measure. Dotted red lines denote ADC. The lines in this graph are for illustration only, as the exact signal changes of different tissues with increasing *b*-values vary and will be contributed by other factors. Note that, liver parenchyma has a T2 of around 40 ms; hepatocellular carcinoma has T2 of around 60 ms; prostate cancer has T2 of around 90 ms, and prostate peripheral zone cancer has T2 of around 170 ms. ADC, apparent diffusion coefficient; IVIM, Intravoxel Incoherent Motion; MRI, magnetic resonance imaging; ms, millisecond; *PF*, perfusion fraction.

Similarly, in a mouse study at 7.0 T with implanted tumors, an increase of the diffusion gradient separation time was associated with an increase of *PF* and a decrease of a D_{slow} variant which considered the non-Gaussian diffusion kurtosis model (*Figure 11*) (33). A mouse brain tissue study at 11.7 T with a triexponential model also showed similar results (*Figure 12*) (34). Thus, Eq. [4] can be re-written as:

$$S(b,TE) = S_0\left(F_{fast}\cdot e^{-TE/T_{2shorter}}\cdot e^{-b\cdot D_{fast}} + F_{slow}\cdot e^{-TE/T_{2longer}}\cdot e^{-b\cdot D_{slow}}\right) \quad [5]$$

Where F_{fast} reflects the compartment portion associated with shorter T2 and F_{slow} reflects the compartment portion associated with longer T2, and (F_{fast} + F_{slow}) =1. For F_{fast}, to be consistent with existing literature, we continue to use the abbreviation *PF*. Thus, *PF* in this letter may also represent the fast signal decay fraction associated with shorter T2 rather than the actual *PF*. It can be seen that, if all other variables can be fixed, then a decrease in shorter T2 corresponds to an increase in *PF* (if only shorter T2 and *PF* are the variables), and an increase in longer T2 corresponds to an increase in D_{slow} (if only longer T2 and D_{slow} are the variables). However, since a change in shorter

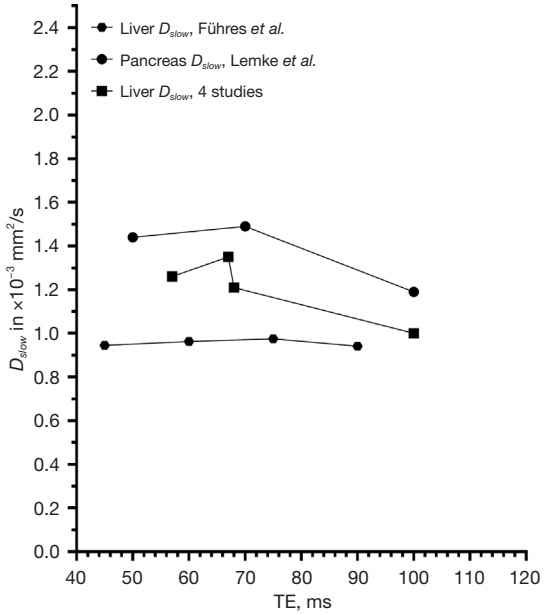

Figure 6 IVIM studies shows, if the TE is increased for data acquisition which can be seen as a reduction of T2, then measured D_{slow} is decreased. The 4 studies data are based on the works of Cercueil *et al.* (17), Kuai *et al.* (18), Wurnig *et al.* (19), and Riexinger *et al.* (20), and these data were listed in the article reported by Riexinger *et al.* (20). Other data are from (13,15). For the 4 studies data, as different data processing methods will lead to different D_{slow} value, the comparison is shown for demonstration only. However, in the study of Riexinger *et al.*, the long TE of 100 ms is likely associated with a truly lower D_{slow} than other studies with shorter TEs. Taking together *Figure 4* and *Figure 6*, it appears that, for TE ranges less than 90 ms, 'longer' TE promotes more *PF* measure than depresses D_{slow} measure. IVIM, Intravoxel Incoherent Motion; ms, millisecond; *PF*, perfusion fraction; TE, time of echo.

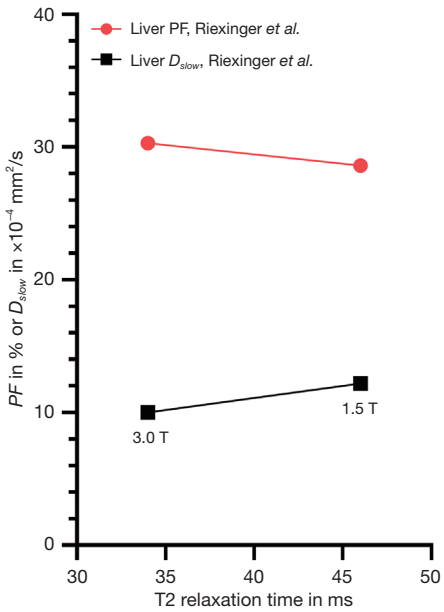

Figure 7 Compared with measures at 1.5 T, liver IVIM measures at 3.0 T are associated with a higher *PF* and lower D_{slow}. The data are based on the work by Riexinger *et al.* (20). This observation, as suggested by the authors (20), may be attributed to the shorter T2 at 3.0 T than at 1.5 T. For demonstration purpose, liver T2 at 1.5 and 3.0 T are assumed to be 46 and 34 ms respectively. Therefore, data in this graph show T2 is negatively associated with *PF* and positively associated with D_{slow}. Similar trends have been reported by other researchers such as the work of Cui *et al.* (21), and reviewed by Li *et al.* (22). IVIM, Intravoxel Incoherent Motion; ms, millisecond; *PF*, perfusion fraction.

T2 or longer T2 can affect other variables such as S_0 and $S_{(b)}$, only experimental studies can further confirm the changes of IVIM parameters caused by T2 change. Note that, during IVIM analysis, we observed that the perfusion compartment and the diffusion compartment are mutually constrained (35-40). For example, the iron deposition and the resulting shorter T2 lead to lower D_{slow} and artificially higher *PF* and D_{fast} in older subjects' liver and spleen than in younger subjects' liver and spleen (35,40). And this may explain younger men's liver has lower D_{slow} and higher *PF* than younger women's liver. Due to the menstrual cycle, pre-menopausal women have lower liver iron level than men. The mutually constrained fast component measure and slow component measure suggests the ratio $S_{(b)}/S_0$ is indeed at least to a degree 'stable'. If $S_{(b)}/S_0$ is 'more stable' or 'with lesser change', then Eq. [5] suggests fast component measure and slow component measure can be negatively correlated (such as an increase of *PF* can be compensated by a decrease of D_{slow} so that $S_{(b)}/S_0$ will be stable).

ADC is the composite of perfusion metrics (*PF* and D_{fast}) and diffusion metric (F_{slow} and D_{slow}). If the 1st *b*-value is 0, and b_2 is the 2nd *b*-value, then from Eq. [2] and Eq. [4], ADC calculation can be approximated according to (ignoring the difference between $T2_{shorter}$ and $T2_{longer}$):

$$ADC = D_{slow} + D_{fast} - b_2^{-1} \ln\left[1 - F_{slow} + \frac{F_{slow}}{e^{-b_2 \cdot (D_{fast})}}\right] \quad [6]$$

Eq. [6] shows ADC is positively correlated with D_{slow} and D_{fast}, and negatively correlated with F_{slow} (thus, positively

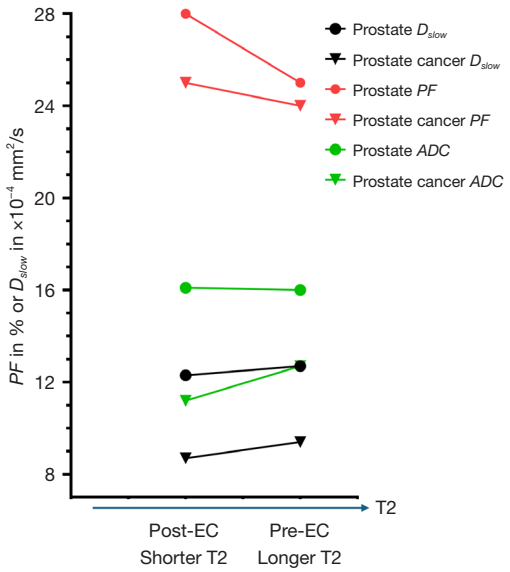

Figure 8 Shortening of prostate peripheral zone and prostate cancer T2 leads to an increase of *PF* and a reduction of D_{slow}, and with a reduction of ADC. The data are from the report by Mazaheri *et al.* (23). Diffusion weighted imaging was conducted before and after administration of a gadolinium agent which shortens T2. The results are consistent with the results shown in *Figures 4*,*6*,*7*. The changes for D_{slow} and ADC are more substantial for cancer tissue, likely due to the greater uptake of gadolinium agent in the cancer tissue than in the normal prostate peripheral zone. The milder changes in D_{slow} still lead to an overall increase in ADC, likely reflecting the large F_{slow}. For both pre-EC and post-EC scans, *PF* is overestimated in this study due to the limited *b*-values applied (23). ADC, apparent diffusion coefficient; EC, enhanced contrast; *PF*, perfusion fraction.

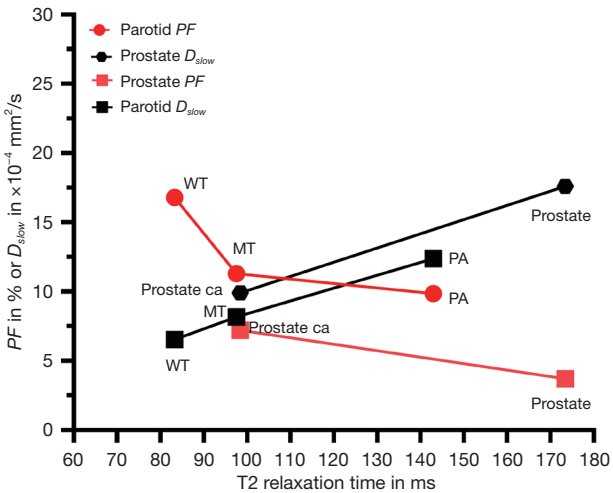

Figure 9 T2 is negatively associated with *PF* and positively associated with D_{slow}. For parotid gland tumors, it is well characterized that PA has long T2 and high ADC, WT has short T2 and low ADC, and the T2 and ADC of MT lie between WT and PA (see *Figure 1*). The parotid tumors T2 values are based on the report by Baohong *et al.* (24), and IVIM measured are based on the report by Ma *et al.* (25). For parotid gland, similar results have been described by other authors such as Yabuuchi *et al.* (26). That tissue perfusion is 'WT > MT > PA' has also been recently described by Yao *et al.* (27). The prostate peripheral zone and prostate cancer T2 values are based on the report by Han *et al.* (28), and IVIM measures are based on the report by Pang *et al.* (29). For prostate, it is well characterized that prostate peripheral zone has long T2 and high ADC, and prostate cancer has shorter T2 and lower ADC. Note that all the tissues in this graph have an aggregate T2 >80 ms; therefore, the slow compartment dominates. Despite the higher *PF* for WT and prostate cancer, still the composite metric of ADC is lower for WT and prostate cancer, likely reflecting the large F_{slow} for these tissues. ADC, apparent diffusion coefficient; ca, cancer; IVIM, Intravoxel Incoherent Motion; ms, millisecond; MT, malignant tumor (parotid gland); *PF*, perfusion fraction; PA, pleomorphic adenoma (parotid gland); WT, Warthin's tumor (parotid gland).

correlated with *PF*).

Figure 5 illustrates that, for tissues with aggregate T2 value <60 ms, if T2 increases from 40 to 60 ms, fast compartment measure decreases while slow compartment measure increases (if we do not consider other contributing factors); however, the decreased measure of fast compartment dominates and the net effect for the composite ADC is a decreased measure. Despite the pathohistological evidence of groupwise higher vasculature in hepatocellular carcinoma (HCC), HCC has been measured paradoxically with a lower *PF* by IVIM (14). For tissues with aggregated T2 value >80 ms, if T2 decreases from 170 to 90 ms, fast compartment measure increases while slow compartment measure decreases (if we do not consider other contributing factors); however, the decrease of the slow compartment dominates and the net effect for the composite ADC is a decreased measure. The observation as shown in *Figure 5* can explain many of the apparently paradoxical observations for ADC measures. For example, articular cartilage has a high ADC of around 1.5×10^{-3} mm^2/s and a T2 of around 37 ms at 3.0 T [see discussion in (4)], thus its high ADC is likely due to its dominant shorter T2 compartment. Chondrosarcoma has a high ADC of around 2.3×10^{-3} mm^2

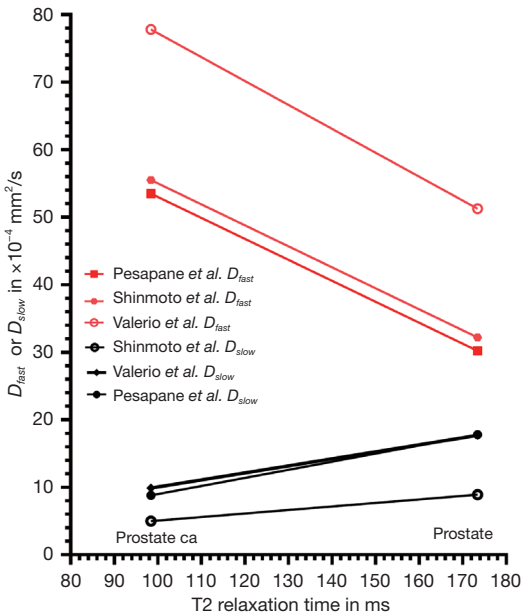

Figure 10 For prostate and prostate cancer, T2 is negatively associated with D_{fast} and positively associated with D_{slow}. Despite the higher D_{fast} for prostate cancer, still the composite metric of ADC is lower for prostate cancer, likely reflecting the large F_{slow} for its tissue. Normal prostate measures are from the peripheral zone. The prostate peripheral zone and prostate cancer T2 values are based on the report by Han *et al.* (28). IVIM data in this graph are based on the reports by Shinmoto *et al.* (30), Valerio *et al.* (31), and Pesapane *et al.* (32). To fit into this graph, the D_{fast} measures reported by Valerio *et al.* are halved in this figure. ca, cancer; ADC, apparent diffusion coefficient; IVIM, Intravoxel Incoherent Motion; ms, millisecond.

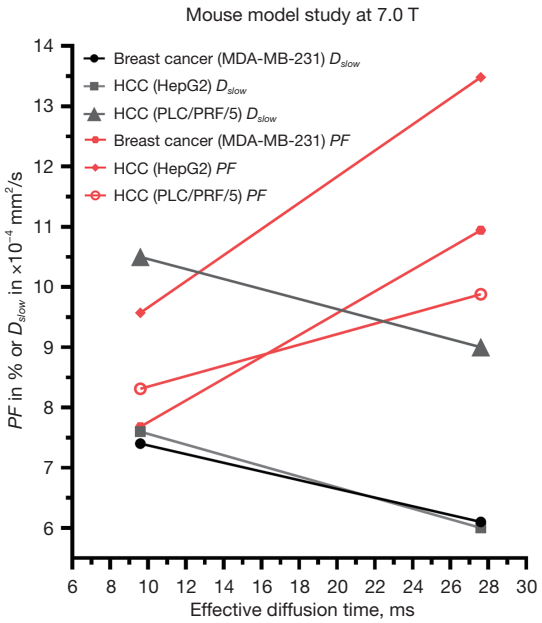

Figure 11 A mouse study at 7.0 T with implanted tumor models shows an increase of the diffusion gradient separation time (effective diffusion time) was associated with an increase of *PF* and a decrease of a D_{slow} variant. The D_{slow} variant was calculated considering the non-Gaussian diffusion kurtosis model. The data are from the report by Iima *et al.* (33). HCC, hepatocellular carcinoma; ms, millisecond; *PF*, perfusion fraction.

and a T2 of around 120 ms [see discussion in (4)], its high ADC measure is likely due to its dominant longer T2 compartment. In the cases of liver lesions, HCC ADC has been noted to have restricted diffusion relative to the liver. However, as HCCs are mostly associated with increased blood supply and increased proportion of arterial blood supply and higher water content (i.e., edema, as shown with higher signal on T2-weighted image and with lower density on X-ray computed tomography), it is unlikely that HCC has true lower diffusion, instead the lower HCC ADC is due to the longer T2 of HCC relative to the liver. Schmid-Tannwald *et al.* (41) reported that the mean ADC value of hypervascular liver metastases was paradoxically lower than the mean ADC value of hypovascular metastases. This could be due to the fact that hypervascular liver metastases have a higher proportion of the longer blood T2 contributed to the lower ADC measure [blood has longer T2 than that of liver metastases, see discussion in (14)].

In addition to T2 (which is often dominant), 'true tissue diffusion' indeed contributes to ADC (2). This is also evidenced by the success of the diffusion tensor imaging technique. When a cluster of voxels has a homogeneous T2 value, then their dominant diffusion direction can still be measured. In addition to the proportions of shorter T2 compartment and longer T2 compartment and 'true tissue diffusion', other factors such as 'true vessel volume' and macroscopic motion also contribute to the composite ADC measure. In an IVIM study of uterine fibroid, after continuous intravenous infusion of oxytocin which is known to decrease uterine fibroid blood flow, Sainio *et al.* (42) reported that all three IVIM parameters (i.e., *PF*, D_{slow}, D_{fast}) of the uterine fibroid decreased. In the case of kidney, kidney ADC is higher than can be predicted by T2, this could be due to the kidney being associated with higher true diffusion and higher true vessel volume [see

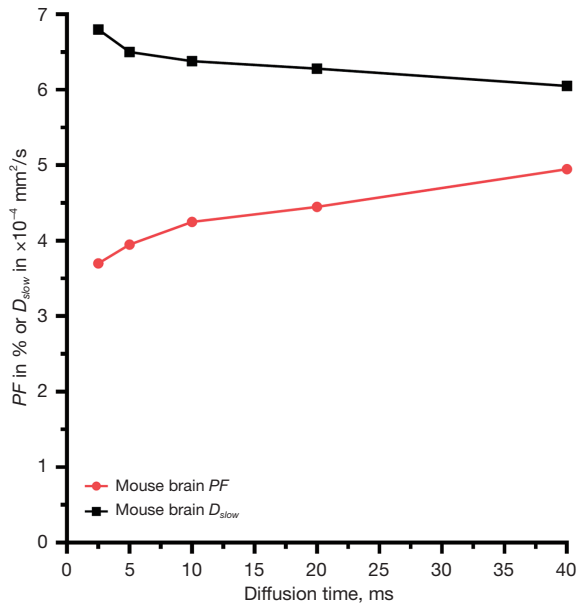

Figure 12 A mouse study at 11.7 T for brain tissue shows an increase of the diffusion gradient separation time (diffusion time) was associated with an increase of *PF* and a decrease of D_{slow}. The data were fitted with a triexponential model. The data are from the report by Wu and Zhang (34). *PF*, perfusion fraction; ms, millisecond.

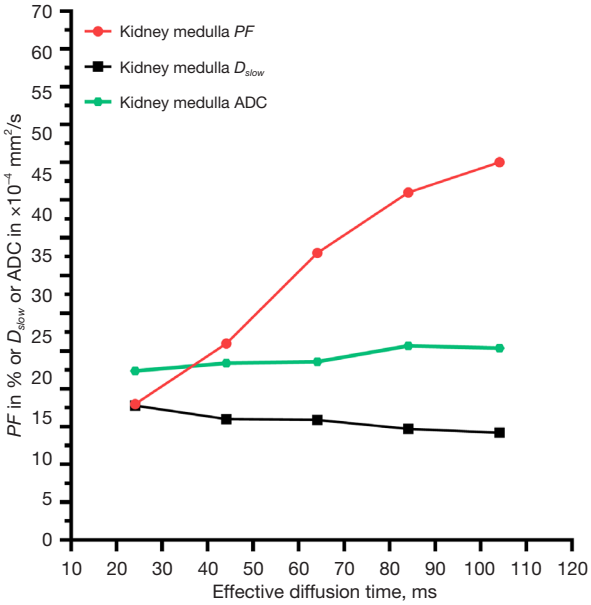

Figure 13 IVIM study at 3.0 T shows, when the effective diffusion time (diffusion gradient separation time) was increased for kidney medulla DWI data acquisition, *PF* increased, D_{slow} decreased, and ADC increased. The kidney cortex diffusion metrics showed the same pattern. Data are from Stabinska *et al.* (44). ADC, apparent diffusion coefficient; DWI, diffusion weighted imaging; IVIM, Intravoxel Incoherent Motion; ms, millisecond; *PF*, perfusion fraction.

discussion in (2)]. Kidney medulla and cortex have a long T2 of around 138 and 121 ms respectively at 3 T (2,43). Recently, Stabinska *et al.* (44) reported that, by increasing the diffusion gradient separation time, the measured kidney medulla and cortex *PF* both increased, while the measured kidney medulla and cortex D_{slow} both decreased, and the net ADC increased (*Figure 13*). In the case of liver aging, there is a shortening of liver T2 (45), a decrease of liver D_{slow} (35), and an artificial increase of liver *PF* and D_{fast} (35). However, the net liver ADC still decreases (46). There could be a decrease of liver true diffusion with aging, and note that there is also a decrease of true vessel volume with aging as measured by histology (47) and by the perfusion metric diffusion derived vessel density (DDVD) (35).

This explanation as shown in *Figure 5* may not apply to *in vitro* studies with phantoms. For example, in a study with phantom, which might have a homogeneous T2 value, Laubach *et al.* (48) did not show a very low ADC measure for the solution with T2 of around 70 ms. Moreover, body fluids also have no perfusion element and their T2 may be 'more homogeneously long'. For the case of gallbladder fluid, ADC is measured higher than can be predicted from T2 (*Figure 1*). Liver cysts are noted to have a higher ADC value than liver hemangioma, though liver hemangiomas are associated with blood flow inside the lesion [for T2 and ADC values see *Figure 14* in (49), also see (50-52)]. Note that liver hemangiomas have a very high DDVD measure while the DDVD of liver cysts is close to zero when properly measured (49,53).

In this letter, we discuss as if ADC is calculated with two *b*-values with the low *b*-value being 0. However, regardless of whether ADC is calculated with *b*=0 or without *b*=0 (such as using *b*=50 and *b*=800 s/mm^2), or with three *b*-values (such as using *b*=0, *b*=50, and *b*=800 s/mm^2), the pattern of triphasic relationship between T2 and ADC always exists (2,4), and the same is true for the relationship between T2 and IVIM parameters (*Figure 14*) (37). If the first *b*-value to calculate the ADC is high, then ADC will be more equivalent to IVIM-D_{slow}. However, D_{slow} values do not appear to be reasonable as well. For example, in a review article by Englund *et al.* (54), it was noted that skeletal muscle has a D_{slow} of 1.46±0.30 mm^2/s which is much higher

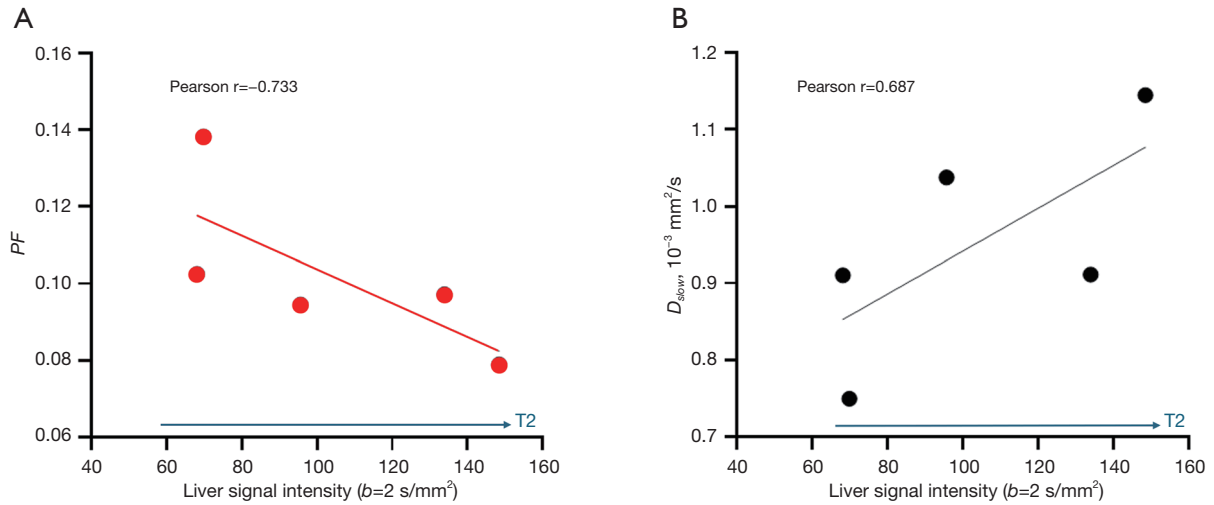

Figure 14 Absolute MR DWI signal intensity (arbitrary unit/pixel) of liver on *b*=2 images and its correlation with D_{slow} and *PF* measure. Five cirrhotic livers' images were acquired at 3 T with 16 *b*-values of 0, 2, 5, 10, 15, 20, 25, 30, 40, 60, 80, 100, 150, 200, 400, and 600 s/mm^2, analyzed by segmented fitting and threshold *b*-value of 60 s/mm^2, with fitting started from *b*=2 s/mm^2 images (*b*=0 image excluded). Stronger liver signal, which can be seen as equivalent to longer T2, is associated with lower *PF* and higher D_{slow}. Adapted from Xiao and Wáng (37). DWI, diffusion weighted imaging; MR, magnetic resonance; ms, millisecond; *PF*, perfusion fraction.

than the liver D_{slow} of 1.1 mm^2/s (20,22). We would think that the D_{slow} of skeletal muscles will not be higher than that of liver with the liver more richly perfused by hepatic artery and portal vein and with lots of sinusoids and space of Disse. Majority of literature reported a lower D_{slow} in HCC tissue than in liver parenchyma (22,55). However, HCC is associated with faster blood transit time and higher free water content than liver parenchyma. Liver fibrosis is associated with longer T2 (2,56), and this longer T2 may depressed *PF* measure and promote D_{slow} measure. We have commented that IVIM measured liver D_{slow} may be too high for severe liver fibrosis patients (39). Both the 'shorter T2 compartment' and 'the longer T2 compartment' consist of a spectrum of varying T2 elements. Though we describe a triphasic dependency of ADC on T2 relaxation time, it is possible that it is actually a biphasic relationship (2). However, due to the ever-existing measurement imprecision and other factors contributing to the ADC, the exact valley bottom of T2 cannot be located. When T2 is around 70 ms, we can assume that the *PF* is very low due to the slower signal decay compared to that when T2 is shorter (such as 30 ms), on the other hand the D_{slow} is also sufficiently low when T2 is 70 ms.

Note that this letter is not a systematic review. Associated with various data processing approaches, the current IVIM literature is highly heterogeneous with varying degrees of data quality. For the fast compartment, the discussion in this letter has been mainly on *PF*, rather than D_{fast}, as D_{fast} is generally more difficult to quantify reliably (16,22). Note that, F_{slow} = (1 – *PF*), and F_{slow} is mostly >0.80 in perfusion/diffusion IVIM observations. In the case of liver, which is richly perfused, its *PF* is around 20% (22). Another point is the discussions on T2 relaxation time in this letter are mostly based on 3-T data.

Diffusion concepts developed from *in vitro* studies may not be applicable to *in vivo* phenomena with heterogeneous T1 and T2 elements. As shown in *Figures 1-3*, *in vivo* ADC measure is more contributed by T2 than by true tissue diffusion, thus we suggest that we do not routinely use the term 'diffusion restriction' when interpreting clinical high *b*-value DW images and ADC maps. Instead, we may choose to use the term 'high signal' on high *b*-value DW image and 'low signal' on ADC map.

Acknowledgments

None.

Footnote

Funding: This work was supported by Hong Kong GRF Project (No. 14112521).

Conflicts of Interest: The author has completed the ICMJE uniform disclosure form (available at https://qims.amegroups.com/article/view/10.21037/qims-2025-195/coif). Y.X.J.W. serves as the Editor-in-Chief of *Quantitative Imaging in Medicine and Surgery*. The author has no other conflicts of interest to declare.

Ethical Statement: The author is accountable for all aspects of the work in ensuring that questions related to the accuracy or integrity of any part of the work are appropriately investigated and resolved.

References

1. Wáng YXJ, Zhao KX, Ma FZ, Xiao BH. The contribution of T2 relaxation time to MRI-derived apparent diffusion coefficient (ADC) quantification and its potential clinical implications. Quant Imaging Med Surg 2023;13:7410-6.
2. Wáng YXJ, Ma FZ. A tri-phasic relationship between T2 relaxation time and magnetic resonance imaging (MRI)-derived apparent diffusion coefficient (ADC). Quant Imaging Med Surg 2023;13:8873-80.
3. Wáng YXJ. The very low magnetic resonance imaging apparent diffusion coefficient (ADC) measure of abscess is likely due to pus's specific T2 relaxation time. Quant Imaging Med Surg 2023;13:8881-5.
4. Wáng YXJ, Aparisi Gómez MP, Ruiz Santiago F, Bazzocchi A. The relevance of T2 relaxation time in interpreting MRI apparent diffusion coefficient (ADC) map for musculoskeletal structures. Quant Imaging Med Surg 2023;13:7657-66.
5. Wáng YXJ. Natural course of apparent diffusion coefficient (ADC) change after brain ischemic stroke: an alternative explanation by the triphasic relationship between T2 and ADC. Quant Imaging Med Surg 2024;14:9848-55.
6. Stadnik TW, Chaskis C, Michotte A, Shabana WM, van Rompaey K, Luypaert R, Budinsky L, Jellus V, Osteaux M. Diffusion-weighted MR imaging of intracerebral masses: comparison with conventional MR imaging and histologic findings. AJNR Am J Neuroradiol 2001;22:969-76.
7. Oh J, Cha S, Aiken AH, Han ET, Crane JC, Stainsby JA, Wright GA, Dillon WP, Nelson SJ. Quantitative apparent diffusion coefficients and T2 relaxation times in characterizing contrast enhancing brain tumors and regions of peritumoral edema. J Magn Reson Imaging 2005;21:701-8.
8. DeMulder D, Ascher SM. Uterine Leiomyosarcoma: Can MRI Differentiate Leiomyosarcoma From Benign Leiomyoma Before Treatment? AJR Am J Roentgenol 2018;211:1405-15.
9. Bura V, Pintican RM, David RE, Addley HC, Smith J, Jimenez-Linan M, Lee J, Freeman S, Georgiu C. MRI findings in-between leiomyoma and leiomyosarcoma: a Rad-Path correlation of degenerated leiomyomas and variants. Br J Radiol 2021;94:20210283.
10. Barral M, Placé V, Dautry R, Bendavid S, Cornelis F, Foucher R, Guerrache Y, Soyer P. Magnetic resonance imaging features of uterine sarcoma and mimickers. Abdom Radiol (NY) 2017;42:1762-72.
11. Egnell L, Jerome NP, Andreassen MMS, Bathen TF, Goa PE. Effects of echo time on IVIM quantifications of locally advanced breast cancer in clinical diffusion-weighted MRI at 3 T. NMR Biomed 2022;35:e4654.
12. Lemke A, Laun FB, Simon D, Stieltjes B, Schad LR. An in vivo verification of the intravoxel incoherent motion effect in diffusion-weighted imaging of the abdomen. Magn Reson Med 2010;64:1580-5.
13. Jerome NP, d'Arcy JA, Feiweier T, Koh DM, Leach MO, Collins DJ, Orton MR. Extended T2-IVIM model for correction of TE dependence of pseudo-diffusion volume fraction in clinical diffusion-weighted magnetic resonance imaging. Phys Med Biol 2016;61:N667-80.
14. Ma FZ, Wáng YXJ. T(2) relaxation time elongation of hepatocellular carcinoma relative to native liver tissue leads to an underestimation of perfusion fraction measured by standard intravoxel incoherent motion magnetic resonance imaging. Quant Imaging Med Surg 2024;14:1316-22.
15. Führes T, Riexinger AJ, Loh M, Martin J, Wetscherek A, Kuder TA, Uder M, Hensel B, Laun FB. Echo time dependence of biexponential and triexponential intravoxel incoherent motion parameters in the liver. Magn Reson Med 2022;87:859-71.

16. Wang YXJ, Huang H, Zheng CJ, Xiao BH, Chevallier O, Wang W. Diffusion-weighted MRI of the liver: challenges and some solutions for the quantification of apparent diffusion coefficient and intravoxel incoherent motion. Am J Nucl Med Mol Imaging 2021;11:107-42.
17. Cercueil JP, Petit JM, Nougaret S, Soyer P, Fohlen A, Pierredon-Foulongne MA, Schembri V, Delhom E, Schmidt S, Denys A, Aho S, Guiu B. Intravoxel incoherent motion diffusion-weighted imaging in the liver: comparison of mono-, bi- and tri-exponential modelling at 3.0-T. Eur Radiol 2015;25:1541-50.
18. Kuai ZX, Liu WY, Zhu YM. Effect of multiple perfusion components on pseudo-diffusion coefficient in intravoxel incoherent motion imaging. Phys Med Biol 2017;62:8197-209.
19. Wurnig MC, Germann M, Boss A. Is there evidence for more than two diffusion components in abdominal organs? - A magnetic resonance imaging study in healthy volunteers. NMR Biomed 2018. doi: 10.1002/nbm.3852.
20. Riexinger AJ, Martin J, Rauh S, Wetscherek A, Pistel M, Kuder TA, Nagel AM, Uder M, Hensel B, Müller L, Laun FB. On the Field Strength Dependence of Bi- and Triexponential Intravoxel Incoherent Motion (IVIM) Parameters in the Liver. J Magn Reson Imaging 2019;50:1883-92.
21. Cui Y, Dyvorne H, Besa C, Cooper N, Taouli B. IVIM Diffusion-weighted Imaging of the Liver at 3.0T: Comparison with 1.5T. Eur J Radiol Open 2015;2:123-8.
22. Li YT, Cercueil JP, Yuan J, Chen W, Loffroy R, Wáng YX. Liver intravoxel incoherent motion (IVIM) magnetic resonance imaging: a comprehensive review of published data on normal values and applications for fibrosis and tumor evaluation. Quant Imaging Med Surg 2017;7:59-78.
23. Mazaheri Y, Hötker AM, Shukla-Dave A, Akin O, Hricak H. Effect of intravascular contrast agent on diffusion and perfusion fraction coefficients in the peripheral zone and prostate cancer. Magn Reson Imaging 2018;51:120-7.
24. Baohong W, Jing Z, Zanxia Z, Kun F, Liang L, Eryuan G, Yong Z, Fei H, Jingliang C, Jinxia Z. T2 mapping and readout segmentation of long variable echo-train diffusion-weighted imaging for the differentiation of parotid gland tumors. Eur J Radiol 2022;151:110265.
25. Ma G, Xu XQ, Zhu LN, Jiang JS, Su GY, Hu H, Bu SS, Wu FY. Intravoxel Incoherent Motion Magnetic Resonance Imaging for Assessing Parotid Gland Tumors: Correlation and Comparison with Arterial Spin Labeling Imaging. Korean J Radiol 2021;22:243-52.
26. Yabuuchi H, Kamitani T, Sagiyama K, Yamasaki Y, Hida T, Matsuura Y, Hino T, Murayama Y, Yasumatsu R, Yamamoto H. Characterization of parotid gland tumors: added value of permeability MR imaging to DWI and DCE-MRI. Eur Radiol 2020;30:6402-12.
27. Yao DQ. King AD, Zhang R, Xiao BH, Wong LM, Wáng YXJ. Assessing parotid gland tumor perfusion with a new imaging biomarker DDVD (diffusion-derived 'vessel density'): initial promising results. Rofo 2025. doi: 10.1055/a-2543-3305.
28. Han D, Choi MH, Lee YJ, Kim DH. Feasibility of Novel Three-Dimensional Magnetic Resonance Fingerprinting of the Prostate Gland: Phantom and Clinical Studies. Korean J Radiol 2021;22:1332-40.
29. Pang Y, Turkbey B, Bernardo M, Kruecker J, Kadoury S, Merino MJ, Wood BJ, Pinto PA, Choyke PL. Intravoxel incoherent motion MR imaging for prostate cancer: an evaluation of perfusion fraction and diffusion coefficient derived from different b-value combinations. Magn Reson Med 2013;69:553-62.
30. Shinmoto H, Tamura C, Soga S, Shiomi E, Yoshihara N, Kaji T, Mulkern RV. An intravoxel incoherent motion diffusion-weighted imaging study of prostate cancer. AJR Am J Roentgenol 2012;199:W496-500.
31. Valerio M, Zini C, Fierro D, Giura F, Colarieti A, Giuliani A, Laghi A, Catalano C, Panebianco V. 3T multiparametric MRI of the prostate: Does intravoxel incoherent motion diffusion imaging have a role in the detection and stratification of prostate cancer in the peripheral zone? Eur J Radiol 2016;85:790-4.
32. Pesapane F, Patella F, Fumarola EM, Panella S, Ierardi AM, Pompili GG, Franceschelli G, Angileri SA, Magenta Biasina A, Carrafiello G. Intravoxel Incoherent Motion (IVIM) Diffusion Weighted Imaging (DWI) in the Periferic Prostate Cancer Detection and Stratification. Med Oncol 2017;34:35.
33. Iima M, Nobashi T, Imai H, Koyasu S, Saga T, Nakamoto Y, Kataoka M, Yamamoto A, Matsuda T, Togashi K. Effects of diffusion time on non-Gaussian diffusion and intravoxel incoherent motion (IVIM) MRI parameters in breast cancer and hepatocellular carcinoma xenograft models. Acta Radiol Open 2018;7:2058460117751565.
34. Wu D, Zhang J. Evidence of the diffusion time dependence of intravoxel incoherent motion in the brain. Magn Reson Med 2019;82:2225-35.

35. Huang H, Zheng CJ, Wang LF, Che-Nordin N, Wáng YXJ. Age and gender dependence of liver diffusion parameters and the possibility that intravoxel incoherent motion modeling of the perfusion component is constrained by the diffusion component. NMR Biomed 2021;34:e4449.
36. Wáng YXJ. Observed paradoxical perfusion fraction elevation in steatotic liver: An example of intravoxel incoherent motion modeling of the perfusion component constrained by the diffusion component. NMR Biomed 2021;34:e4488.
37. Xiao BH, Wáng YXJ. Different tissue types display different signal intensities on b = 0 images and the implications of this for intravoxel incoherent motion analysis: Examples from liver MRI. NMR Biomed 2021;34:e4522.
38. Wáng YXJ. A reduction of perfusion can lead to an artificial elevation of slow diffusion measure: examples in acute brain ischemia MRI intravoxel incoherent motion studies. Ann Transl Med 2021;9:895.
39. Wáng YXJ. Mutual constraining of slow component and fast component measures: some observations in liver IVIM imaging. Quant Imaging Med Surg 2021;11:2879-87.
40. Yu WL, Ma FZ, Huang H, Xiao BH, Li XM, Wáng YXJ. Age and gender differences of normative values of spleen diffusion MRI parameters. Rofo 2024. [Epub ahead of print]. doi: 10.1055/a-2357-9741.
41. Schmid-Tannwald C, Thomas S, Ivancevic MK, Dahi F, Rist C, Sethi I, Oto A. Diffusion-weighted MRI of metastatic liver lesions: is there a difference between hypervascular and hypovascular metastases? Acta Radiol 2014;55:515-23.
42. Sainio T, Saunavaara J, Komar G, Viitala A, Otonkoski S, Joronen K, Perheentupa A, Sequeiros RB. Assessing blood flow in uterine fibroids using intravoxel incoherent motion imaging compared with dynamic contrast-enhanced MRI. Sci Rep 2025;15:2980.
43. Li X, Bolan PJ, Ugurbil K, Metzger GJ. Measuring renal tissue relaxation times at 7 T. NMR Biomed 2015;28:63-9.
44. Stabinska J, Thiel TA, Zöllner HJ, Benkert T, Wittsack HJ, Ljimani A. Investigation of diffusion time dependence of apparent diffusion coefficient and intravoxel incoherent motion parameters in the human kidney. Magn Reson Med 2024. [Epub ahead of print]. doi: 10.1002/mrm.30396.
45. Schwenzer NF, Machann J, Haap MM, Martirosian P, Schraml C, Liebig G, Stefan N, Häring HU, Claussen CD, Fritsche A, Schick F. T2* relaxometry in liver, pancreas, and spleen in a healthy cohort of one hundred twenty-nine subjects-correlation with age, gender, and serum ferritin. Invest Radiol 2008;43:854-60.
46. Metens T, Ferraresi KF, Farchione A, Moreno C, Bali MA, Matos C. Normal hepatic parenchyma visibility and ADC quantification on diffusion-weighted MRI at 3 T: influence of age, gender, and iron content. Eur Radiol 2014;24:3123-33.
47. Fiel MI, Deniz K, Elmali F, Schiano TD. Increasing hepatic arteriole wall thickness and decreased luminal diameter occur with increasing age in normal livers. J Hepatol 2011;55:582-6.
48. Laubach HJ, Jakob PM, Loevblad KO, Baird AE, Bovo MP, Edelman RR, Warach S. A phantom for diffusion-weighted imaging of acute stroke. J Magn Reson Imaging 1998;8:1349-54.
49. Hu GW, Li CY, Zhang G, Zheng CJ, Ma FZ, Quan XY, Chen W, Sabarudin A, Zhu MSY, Li XM, Wáng YXJ. Diagnosis of liver hemangioma using magnetic resonance diffusion-derived vessel density (DDVD) pixelwise map: a preliminary descriptive study. Quant Imaging Med Surg 2024;14:8064-82.
50. Fenlon HM, Tello R, deCarvalho VL, Yucel EK. Signal characteristics of focal liver lesions on double echo T2-weighted conventional spin echo MRI: observer performance versus quantitative measurements of T2 relaxation times. J Comput Assist Tomogr 2000;24:204-11.
51. Cittadini G, Santacroce E, Giasotto V, Rescinito G. Focal liver lesions: characterization with quantitative analysis of T2 relaxation time in TSE sequence with double echo time. Radiol Med 2004;107:166-73.
52. Tokgoz O, Unlu E, Unal I, Serifoglu I, Oz I, Aktas E, Caglar E. Diagnostic value of diffusion weighted MRI and ADC in differential diagnosis of cavernous hemangioma of the liver. Afr Health Sci 2016;16:227-33.
53. Ju ZG, Leng XM, Xiao BH, et al. Influences of the second motion probing gradient b-value and T2 relaxation time on magnetic resonance diffusion-derived 'vessel density' (DDVD) calculation: the examples of liver, spleen, and liver simple cyst. Quant Imaging Med Surg 2025;15:74-87.
54. Englund EK, Reiter DA, Shahidi B, Sigmund EE. Intravoxel Incoherent Motion Magnetic Resonance Imaging in Skeletal Muscle: Review and Future Directions. J Magn Reson Imaging 2022;55:988-1012.
55. Yue X, Lu Y, Jiang Q, Dong X, Kan X, Wu J, Kong X, Han P, Yu J, Li Q. Application of Intravoxel Incoherent Motion in the Evaluation of Hepatocellular Carcinoma

after Transarterial Chemoembolization. Curr Oncol 2022;29:9855-66.
56. Guimaraes AR, Siqueira L, Uppal R, Alford J, Fuchs BC, Yamada S, Tanabe K, Chung RT, Lauwers G, Chew ML, Boland GW, Sahani DV, Vangel M, Hahn PF, Caravan P. T2 relaxation time is related to liver fibrosis severity. Quant Imaging Med Surg 2016;6:103-14.

Cite this article as: Wáng YXJ. An explanation for the triphasic dependency of apparent diffusion coefficient (ADC) on T2 relaxation time: the multiple T2 compartments model. Quant Imaging Med Surg 2025;15(4):3779-3791. doi: 10.21037/qims-2025-195

